Energy Fuels **2010,** *24,* 888–896 · DOI:10.1021/ef901047r
Published on Web 12/15/2009

energy&fuels
article

Modeling the Auto-Ignition of Oxygenated Fuels using a Multistep Model

Elisa Toulson,*,† Casey M. Allen,† Dennis J. Miller,‡ and Tonghun Lee†

†*Department of Mechanical Engineering, Michigan State University, 2555 Engineering Building, East Lansing, Michigan 48824 and* ‡*Department of Chemical Engineering and Material Science, Michigan State University, 2557 Engineering Building, East Lansing, Michigan 48824*

Received September 16, 2009. Revised Manuscript Received November 12, 2009

The research presented here describes the application of a multistep (8-step) autoignition model to oxygenated fuels such as alcohols and esters in a rapid compression machine. This modeling concept is aimed at capturing the ignition behavior of new oxygenated fuel blends, where detailed or reduced chemical kinetics data are not available. The predicted ignition delays from the multistep autoignition model using the biodiesel surrogate fuel methyl butanoate are validated against results attained using a detailed chemical kinetic mechanism (Dooley, S.; Curran, H.J.; Simmie, J.M. *Combust. Flame* **2008**, *153* (1−2), 2−32.) in conjunction with CHEMKIN. Once the multistep model constants were calibrated for methyl butanoate, the model showed good agreement with the detailed mechanism ignition delays, but with significantly reduced computational time. The multistep model was tested over a compressed temperature range of 750−925 K, compressed pressures from 10 to 46 atm and equivalence ratios from 0.5 to stoichiometric, with the percent relative error in the ignition delay between the multistep and CHEMKIN modeling found to be less than 15%.

Introduction

Biofuels are presently receiving much attention as they are renewable, carbon neutral, and provide energy security in comparison to their fossil fuel counterparts.[2,3] Several different liquid and gaseous fuels derived from biomass are being researched for use in the transportation sector.[4] These fuels include biodiesel,[4−7] bioethanol,[4,8,9] biomethanol,[10,11] biohydrogen,[3,12,13] and biosyngas-derived Fischer−Tropsch Synthesis fuels.[14−17]

Alcohols created from fermentation processes and methyl-esters produced by the transesterification of raw vegetable oil with an alcohol are generally regarded as first generation biofuels.[18] The most successful biofuels generated from these processes are ethanol and biodiesel, which can be used neat or in blends with their petroleum-based counterparts, gasoline and diesel, with only minor modifications to current engines.[19,20]

Over the years, much effort has been made to understand the detailed chemical kinetics for both ethanol and biodiesel, with varying degrees of progress. Due to the simple nature of ethanol, its chemical kinetics are relatively well-known and several detailed kinetic mechanisms exist;[21−23] however, further work remains, especially in modeling chemistry at high pressures.[23]

Biodiesels are generally composed of a mixture of multiple monoalkyl esters of long-chain fatty acids (∼12−18 carbon atoms) made most commonly from soy or rapeseed oil by transesterification with an alcohol.[2,24] There has been limited development of detailed chemical kinetic models of biodiesel molecules due to their large size, although a recent study describes a kinetic mechanism for methyl decanoate.[24]

*To whom correspondence should be addressed. E-mail: toulson@msu.edu. Phone: (517) 884-1547.

(1) Dooley, S.; Curran, H. J.; Simmie, J. M. *Combust. Flame* **2008**, *153* (1−2), 2–32.
(2) Westbrook, C. K.; Pitz, W. J.; Westmoreland, P. R.; Dryer, F. L.; Chaos, M.; Osswald, P.; Kohse-Höinghaus, K.; Cool, T. A.; Wang, J.; Yang, B.; Hansen, N.; Kasper, T. *Proc. Combust. Inst.* **2009**, *32* (1), 221–228.
(3) Demirbas, A. *Energy Convers. Manage.* **2008**, *49* (8), 2106–2116.
(4) Demirbas, A. *Prog. Energy Combust. Sci.*, 2007. *33*(1).
(5) Lapuerta, M.; Armas, O.; Rodríguez-Fernández, J. *Prog. Energy Combust. Sci.* **2008**, *34* (2), 198–223.
(6) Shahid, E. M.; Jamal, Y. *Renewable Sustainable Energy Rev.* **2008**, *12* (9), 2484–2494.
(7) Demirbas, A. *Energy Convers. Manage.* **2009**, *50* (1), 14–34.
(8) Balat, M.; Balat, H. *Applied Energy* **2009**, *86* (11), 2273–2282.
(9) Gnansounou, E.; Dauriat, A.; Villegas, J.; Panichelli, L. *Bioresour. Technol.* **2009**, *100* (21), 4919–4930.
(10) Hasegawa, F.; Yokoyama, S.; Imou, K. *Bioresour. Technol.* In Press.
(11) Lim, K. O.; Sims, R. E. H. *Liquid and Gaseous Biomass Fuels Bioenergy Options for a Cleaner Environment*; Elsevier: Oxford, 2004; pp 103−140.
(12) Meher Kotay, S.; Das, D. *Int. J. Hydrogen Energy IWHE 2006* **2008**, *33* (1), 258–263.
(13) Liu, X.; Ren, N.; Song, F.; Yang, C.; Wang, A. *Prog. Nat. Sci.* **2008**, *18* (3), 253–258.
(14) Tijmensen, M. J. A.; Faaij, A. P. C.; Hamelinck, C. N.; van Hardeveld, M. R. M. *Biomass Bioenergy* **2002**, *23* (2), 129–152.
(15) Jun, K.-W.; Roh, H.-S.; Kim, K.-S.; Ryu, J.-S.; Lee, K.-W. *Appl. Catal., A* **2004**, *259* (2), 221–226.
(16) Takeshita, T.; Yamaji, K. *Energy Policy* **2008**, *36* (8), 2773–2784.
(17) Prins, M. J.; Ptasinski, K. J.; Janssen, F. J. J. G. *Fuel Process. Technol.* **2005**, *86* (4), 375–389.
(18) Fatih Demirbas, M. *Appl. Energy Biofuels Asia* **2009**, *86* (Supplement 1), S151–S161.
(19) Demirbas, A. *Energy Policy* **2007**, *35* (9), 4661–4670.
(20) Demirbas, A. *Appl. Energy Biofuels Asia* **2009**, *86* (Supplement 1), S108–S117.
(21) Marinov, N. M. *Int. J. Chem. Kinetics* **1999**, *31*, 183–220.
(22) Li, J. D.; Kazakov, A.; Chaos, M.; Dryer, F. L. Chemical Kinetics of Ethanol Oxidation. in *5th US Combustion Meeting*, 2007; Western States Section of the Combustion Institute.
(23) Saxena, P.; Williams, F. A. *Combust. Flame* **2006**, *145* (1−2), 316–323.
(24) Herbinet, O.; Pitz, W. J.; Westbrook, C. K. *Combust. Flame* **2008**, *154* (3), 507–528.

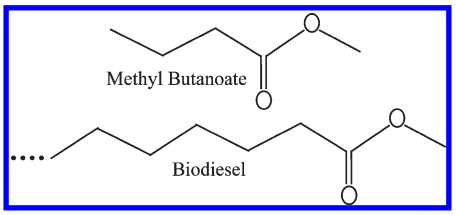

Figure 1. Chemical structures of methyl butanoate and biodiesel.[32]

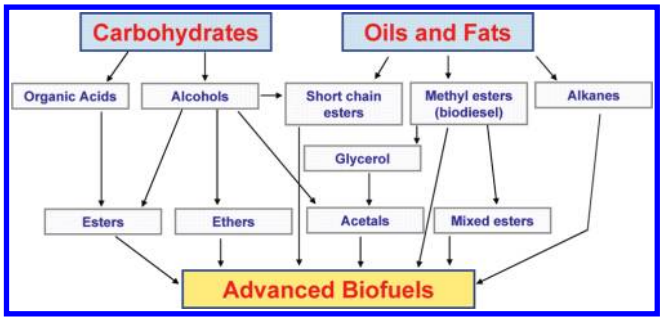

Figure 2. Formation routes for second generation biofuels from both plant carbohydrates and lipids.

Research often focuses on small alkyl esters such as methyl butanoate and ethyl propionate,[1,2,24−31] which are considered biodiesel surrogates because they contain much of the same chemical structure of their larger counterparts (Figure 1) but with a chemical mechanism of a more manageable size.[32] The chemistry of biodiesels is much less well understood than that of traditional fossil fuels, as their chemical structure is considerably different due to the oxygen atoms present in the alkyl chain.[1]

Currently, a collective effort is underway to seek a new generation of advanced biofuels that are produced by advanced thermochemical processes to optimize yields and promote sustainable growth.[18,19] These next generation biofuels are formulated by blending a variety of renewable, organic components that are derived from carbohydrates and from oils and fats to actively optimize physical properties and combustion characteristics, as described in Figure 2.[4,19] Since next generation biofuels are blended from many different components, no detailed kinetic mechanisms are readily available. For this reason, the work described here focuses on using a multistep modeling approach to simulate the ignition of both biofuels and their blends.

Rapid compression machines (RCM) are commonly used for homogeneous chemical kinetics studies at engine relevant pressure−temperature conditions. The Michigan State University RCM incorporates a creviced piston to reduce complicated fluid mechanics and near-wall mixing inside the combustion chamber, in order to improve the postcompression temperature distribution in the combustion chamber and achieve a homogeneous core region and accurate characterization of mixture temperatures for kinetic studies.[33−35] With RCMs it is desirable to heat the test fuel mixture as rapidly as possible to a high temperature and pressure with minimal heat losses. For this reason, although the Michigan State University RCM compression time is near 30 ms, ~50% of the compression occurs in the last 3 ms (Figure 5), which minimizes the chemistry that occurs during the compression stroke. Minimizing the chemistry during this period is important as this reduces the formation of radical species and heat release that may later affect the ignition delay. Recently, Mittal et al.[36] published an RCM kinetic modeling study in which they indicate that it is important to model the chemistry during the compression stroke, as is done in this work, in order to accurately predict the ignition delay.

Motivation

At present, there is a high computational cost when incorporating a detailed kinetic mechanism into a computational fluid dynamic (CFD) model. To reduce computational time, a multistep ignition model such as that introduced by Halstead et al.[37] can be employed in place of the detailed chemical kinetics. With a multistep model, the reaction steps are empirical and consequently only describe the overall behavior of the detailed kinetics.[38] Because of this, the kinetic parameters may require modification if the model is used with different fuels, fuel blends, or even isomers of the same fuel.

The main benefit of this type of modeling is to capture the ignition behavior of novel blends of oxygenated compounds, for which no detailed kinetics data are available. The multistep model maintains the flexibility to model complex ignition trends that are impossible to capture using a single global reaction model that is incapable of accommodating both low and high temperature regions.[39−42] To predict the combustion process out to the equilibrium state, as is required in CFD applications, the multistep ignition model must be coupled with a combustion model such as that used by Yuan et al.[41] or Sazhina et al.[42] With this type of combustion model, when the temperature of a cell is greater than 1100 K or when a very sharp temperature rise ($> 10^7$ K/s) occurs in a cell of the CFD model, the shell ignition model is inhibited and the high temperature combustion model takes over.[42]

(25) Hayes, C. J.; Burgess, D. R., Jr. *Proc. Combust. Inst.* **2009**, *32* (1), 263–270.
(26) Gaïl, S.; Sarathy, S. M.; Thomson, M. J.; Diévart, P.; Dagaut, P. *Combust. Flame* **2008**, *155* (4), 635–650.
(27) HadjAli, K.; Crochet, M.; Vanhove, G.; Ribaucour, M.; Minetti, R. *Proc. Combust. Inst.* **2009**, *32* (1), 239–246.
(28) Fisher, E. M.; Pitz, W. J.; Curran, H. J.; Westbrook, C. K. *Proc. Combust. Inst.* **2000**, *28*, 1579–1586.
(29) Metcalfe, W. K.; Dooley, S.; Curran, H. J.; Simmie, J. M.; El-Nahas, A. M.; Navarro, M. V. *J. Phys. Chem. A* **2007**, *111*, 4001–4014.
(30) Farooq, A.; Davidson, D. F.; Hanson, R. K.; Huynh, L. K.; Violi, A. *Proc. Combust. Inst.* **2009**, *32* (1), 247–253.
(31) Gaïl, S.; Thomson, M. J.; Sarathy, S. M.; Syed, S. A.; Dagaut, P.; Diévart, P.; Marchese, A. J.; Dryer, F. L. *Proc. Combust. Inst.* **2007**, *31* (1), 305–311.
(32) Westbrook, C. K.; Pitz, W. J.; Curran, H. J. *J. Phys. Chem. A* **2006**, *110* (21), 6912–6922.
(33) Mittal, G.; Sung, C. J. *Combust. Sci. Technol.* **2007**, *179* (3), 497–530.
(34) Lee, D.; Hochgreb, S. *Combust. Flame* **1998**, *114* (3−4), 531–545.
(35) Brett, L.; Macnamara, J.; Musch, P.; Simmie, J. M. *Combust. Flame* **2001**, *124* (1−2), 326–329.
(36) Mittal, G.; Chaos, M.; Sung, C.-J.; Dryer, F. L. *Fuel Processing Technology Dimethyl Ether Special Section* **2008**, *89* (12), 1244–1254.
(37) Halstead, M. P.; Kirsch, L. J.; Quinn, C. P. *Combust. Flame* **1977**, *30*, 45–60.
(38) Hamosfakidis, V.; Reitz, R. D. *Combust. Flame* **2003**, *132* (3), 433–450.
(39) Zheng, J.; Yang, W.; Miller, D. L.; Cernansky, N. A Global Reaction Model for the HCCI Combustion Process. In *2002 Spring Meeting of the Western States Section of the Combustion Institute*, San Diego, CA, 2002.
(40) Yuan, W.; Hansen, A. C.; Zhang, Q. Computational Study of Biodiesel Ignition in a Direct Injection Engine. In *ASAE Annual International Meeting*; Las Vegas, Nevada, USA, 2003.
(41) Yuan, W.; Hansen, A. C.; Tat, M. E.; Van Gerpen, J. H.; Tan, Z. *Tranactions of the ASAE* **2005**, *48* (3), 933–939.
(42) Sazhina, E. M.; Sazhin, S. S.; Heikal, M. R.; Marooney, C. J. *Fuel* **1999**, *78* (4), 389–401.

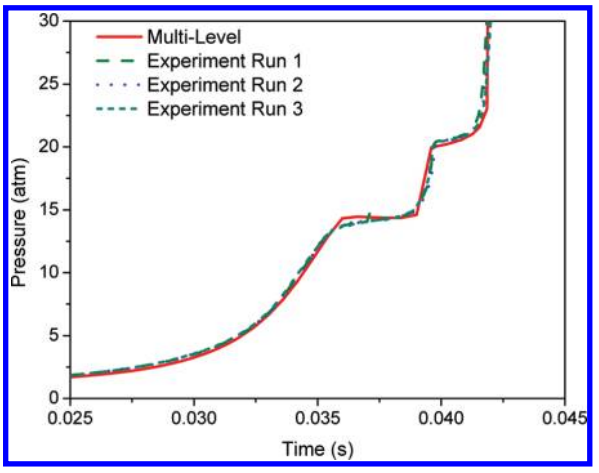

Figure 3. Di-butyl ether experimental RCM pressure traces and multistep modeling results showing 2-stage ignition (compression ratio 7.75, $T_0 = 295$ K, $P_0 = 1$ atm).

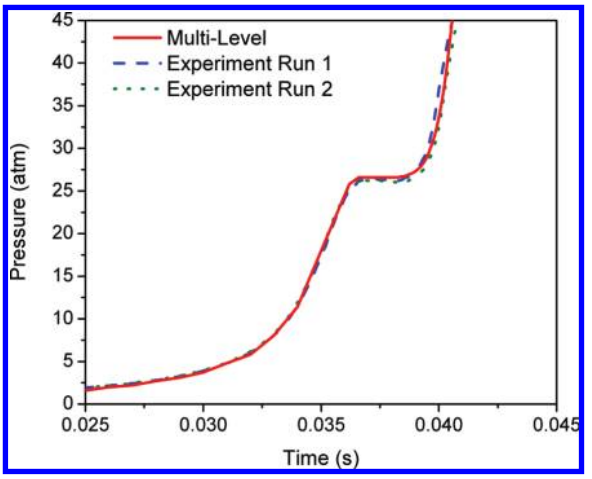

Figure 4. Ethanol experimental RCM pressure traces and multistep modeling results showing single-stage ignition (compression ratio 17, $T_0 = 343$ K, $P_0 = 0.8$ atm).

Examples of the adaptation of the multilevel model to both single- and two-stage ignition fuels are shown in Figures 3 and 4 (solid line), which also show dibutyl ether and ethanol RCM experimental runs (dashed line) performed in the Michigan State University RCM.[43]

The focus of this study is to demonstrate the use of this type of multistep model for predicting autoignition of oxygenated fuels in a RCM, with validation through the comparison of results attained with a detailed chemical kinetics model. Methyl butanoate was chosen as the test fuel because a detailed chemical mechanism for this oxygenated fuel is available, which has been validated over conditions encountered in a RCM.[1]

Multistep Ignition Model

The multistep kinetics ignition model used for this work is based on the Shell Model of Halstead et al.,[37,44] which was originally designed to predict hydrocarbon autoignition (knock) in gasoline engines. More recently, the model has also been shown to be applicable to diesel and biodiesel ignition in compression ignition engines.[40−42,45,46] The model developed by Halstead et al.[37] is shown in Table 1 and consists of seven species (five generic, O_2, and N_2) and eight reactions that are based on the degenerate chain branching characteristic of hydrocarbon autoignition. In addition, the model contains 26 constants that are unique to a particular fuel. For this work the model was modified to accommodate oxygenated hydrocarbons. The species involved in the multistep kinetic model adapted to oxygenated hydrocarbons are: (1) RH, the hydrocarbon fuel of composition $C_nH_{2n}O_k$; (2) O_2, oxygen; (3) R*, the radical formed from the fuel; (4) B, the branching agent; (5) Q, the intermediate species; (6) P, the products (CO, CO_2 and H_2O); (7) N_2, nitrogen.

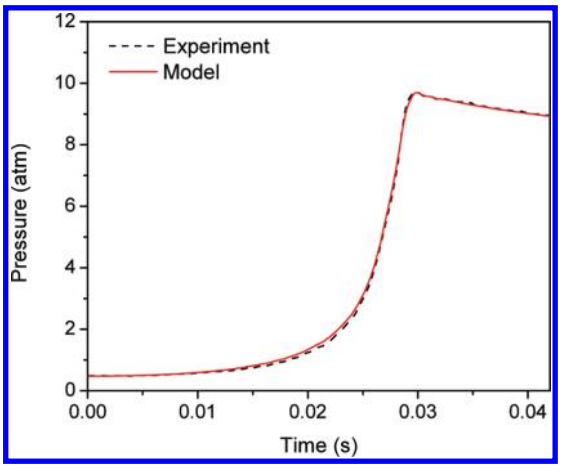

Figure 5. Comparison of experimental (dashed) and simulated pressure traces for a nonreactive mixture ($P_0 = 0.5$ atm, $T_0 = 297$ K).

Table 1. Autoignition Reaction Mechanism[37]

	step	reaction	rate coefficient
1	initiation	$RH + O_2 \rightarrow 2R^*$	k_q
2	propagation	$R^* \rightarrow R^* + P + \text{Heat}$	k_p
3	propagation	$R^* \rightarrow R^* + B$	$f_1 k_p$
4	propagation	$R^* \rightarrow R^* + Q$	$f_4 k_p$
5	propagation	$R^* + Q \rightarrow R^* + B$	$f_2 k_p$
6	branching	$B \rightarrow 2R^*$	k_b
7	termination	$R^* \rightarrow$ termination	$f_3 k_p$
8	termination	$2R^* \rightarrow$ termination	k_t

The rate terms f_i ($i = 1, 2, 3$ and 4) are expressed as functions of the fuel and oxygen concentrations as:

$$f_i = A_{f_i} \exp\left(\frac{-E_{f_i}}{RT}\right)[O_2]^{x_i}[RH]^{y_i} \quad (1)$$

The kinetic parameters k_i (i = p1, p2, p3, b, and t) are in the Arrhenius form:

$$k_i = A_i \exp\left(\frac{-E_i}{RT}\right) \quad (2)$$

with the exception of k_p which is given by:

$$k_p = \left(\frac{1}{k_{p_1}[O_2]} + \frac{1}{k_{p_2}} + \frac{1}{k_{p_3}[RH]}\right)^{-1} \quad (3)$$

The intermediate species (Q), formed in reaction 4, represents oxygenated compounds such as aldehydes (RCHO)

(43) Allen, C. M.; Lee, T. *Energetic-Nanoparticle-Enhanced Combustion of Liquid Fuels in a Rapid Compression Machine*. In *47th AIAA Aerospace Science Meeting*, Orlando, FL, 2009; AIAA: 2009; p 227.
(44) Halstead, M. P.; Kirsch, L. J.; Prothero, A.; Quinn, C. P.; Proc, R. *Soc. Lond. A* **1975**, *346*, 515–538.
(45) Kong, S.-C.; Han, Z.; Reitz, R. D. SAE Paper 950278, 1995.
(46) Kong, S.-C.; Reitz, R. D. *J. Eng. Gas Turbines Power* **1993**, *115*, 781–789.

during the first induction period and the alkylperoxy radical (RO_2) and its isomerization products during the second induction period.[45] These intermediate species are capable of enhancing the rate of formation of the degenerate branching intermediate (B) in reaction 5.[47] The branching intermediate is related to hydroperoxide (RO_2H) at low temperature and hydrogen peroxide (H_2O_2) at high temperature.[48]

If two hydrogen atoms are abstracted per propagation cycle from the hydrocarbon fuel molecule with the structure, C_nH_{2m}, the amount of fuel consumed per cycle is $1/m$ or $C_{n/m}H_2$. The main reaction can therefore be written as:

$$C_{n/m}H_2 + pO_2 \rightarrow \frac{n\gamma}{m}CO + \frac{n(1-\gamma)}{m}CO_2 + H_2O \quad (4)$$

The coefficient γ determines the burned product mixture where

$$\frac{CO}{CO_2} = \frac{\gamma}{1-\gamma} \quad (5)$$

with $\gamma = 0.67$ in the original ignition model by Halstead et al.[37]

The oxygen consumption p for a hydrocarbon is:

$$p = \frac{n(2-\gamma) + m}{2m} \quad (6)$$

For an oxygenated hydrocarbon with the structure $C_nH_{2m}O_k$, the amount of fuel consumed per cycle is $C_{n/m}H_2O_{k/m}$, and the main combustion reaction can be written as:

$$C_{n/m}H_2O_{k/m} + pO_2 \rightarrow \frac{n\gamma}{m}CO + \frac{n(1-\gamma)}{m}CO_2 + H_2O \quad (7)$$

where the oxygen consumption p for an oxygenated hydrocarbon is:

$$p = \frac{n(2-\gamma) + m - k}{2m} \quad (8)$$

In order to remove the fixed CO/CO_2 assumption, as this is a function of the stoichiometry of the reactants, Hamosfakidis and Reitz[38] altered the original reaction to:

$$\frac{1}{m}C_nH_{2m} + p(O_2 + c_{N_2}N_2 + c_{H_2O}H_2O + c_{CO_2}CO_2) \rightarrow v_{C_nH_{2m}}C_nH_{2m} + v_{CO}CO + v_{CO_2}CO_2 + v_{H_2O}H_2O + v_{O_2}O_2 + v_{N_2}N_2 + v_{H_2}H_2 \quad (9)$$

where

$$p = \frac{(n/m + 1/2)}{\phi} \quad (10)$$

and ϕ is the equivalence ratio.

For an oxygenated hydrocarbon the removal of the fixed CO/CO_2 assumption is also important as methyl esters are known to produce CO_2 directly from decomposition of the ester.[49] Therefore, for an oxygenated hydrocarbon the reaction becomes:

$$\frac{1}{m}C_nH_{2m}O_k + p(O_2 + c_{N_2}N_2 + c_{H_2O}H_2O + c_{CO_2}CO_2) \rightarrow v_{C_nH_{2m}O_k}C_nH_{2m}O_k + v_{CO}CO + v_{CO_2}CO_2 + v_{H_2O}H_2O + v_{O_2}O_2 + v_{N_2}N_2 + v_{H_2}H_2 \quad (11)$$

where

$$p = \frac{(n/m + 1/2 - k/2m)}{\phi} \quad (12)$$

One of the main deficiencies of the original model by Halstead et al.[37] is that it violates mass conservation. To maintain mass conservation, Schapertons and Lee[50] modified the propagation sequence so that the depletion of fuel and oxygen per propagation cycle is increased to account for the production of Q and B, which are generated at rates proportional to the production cycle. To accomplish this the main propagation cycle (reactions 2−4), with reaction rate k_pR^*, was rewritten as:

$$R^* + (\Lambda + 1)\left(\frac{1}{m}C_nH_{2m} + pO_2\right) \rightarrow qP + f_1B + f_4Q + R^* + \text{Heat} \quad (13)$$

where

$$\Lambda = \frac{f_1MW_B + f_4MW_Q}{MW_{RH}/m + pMW_{O_2}} \quad (14)$$

MW_x is the molecular weight of the species x,

$$p = \frac{(n/m + 1/2)}{\phi} \quad (15)$$

and

$$q = 1 + n/m \quad (16)$$

For an oxygenated hydrocarbon this becomes:

$$R^* + (\Lambda + 1)\left(\frac{1}{m}C_nH_{2m}O_k + pO_2\right) \rightarrow qP + f_1B + f_4Q + R^* + \text{Heat} \quad (17)$$

where

$$\Lambda = \frac{f_1MW_B + f_4MW_Q}{MW_{RH}/m + pMW_{O_2}} \quad (18)$$

$$p = \frac{(n/m + 1/2 - k/2m)}{\phi} \quad (19)$$

and

$$q = 1 + n/m + p(1-\phi) \quad (20)$$

The two termination reactions 7 and 8 were also altered to maintain mass conservation by converting radicals into inert species, instead of ignoring their contribution to the mass balance.[50] Reactions 7 and 8 were therefore rewritten as:

$$R^* \rightarrow \frac{MW_{R^*}}{MW_{N_2}}N_2 \quad (21)$$

$$2R^* \rightarrow 2\frac{MW_{R^*}}{MW_{N_2}}N_2 \quad (22)$$

These two radical termination reactions were further modified by Hamosfakidis and Reitz[38] so that combustion products,

(47) Griffiths Prog. Energy Combust. Sci., **1995**, *21*, 25−107.
(48) Benson, S. W. Prog. Energy Combust. Sci. **1981**, *7*, 125.
(49) Biet, J.; Warth, V.; Herbinet, O.; Glaude, P. A.; Battin-Leclerc, F. *Proceedings of the European Combustion Meeting*, 2009.
(50) Schapertons, H.; Lee, W. *SAE Paper 850502*, 1985.

rather than N_2, were produced from the termination of the radical species.

$$R* \rightarrow \frac{MW_{R*}}{MW_P}P \quad (23)$$

$$2R* \rightarrow 2\frac{MW_{R*}}{MW_P}P \quad (24)$$

Where the products (P) of the combustion of an oxygenated hydrocarbon are:

$$P = v_{C_nH_{2m}O_k}C_nH_{2m}O_k + v_{CO}CO + v_{CO_2}CO_2 + v_{H_2O}H_2O + v_{O_2}O_2 + v_{H_2}H_2 \quad (25)$$

For the lean to stoichiometric combustion used for this research this can be further reduced to:

$$P = v_{CO_2}CO_2 + v_{H_2O}H_2O + v_{O_2}O_2 \quad (26)$$

Mass balancing is accomplished by defining the molecular weights (MW) of the five generic species.[50] For the lean to stoichiometric combustion of an oxygenated hydrocarbon the molecular weights are defined by the following equations:
Fuel

MW_{RH} depends on the fuel structure $C_nH_{2m}O_k$:

$$MW_{RH} = n(12.0108) + 2m(1.0079) + k(15.9994) \quad (27)$$

Radicals

$$MW_{R*} = (MW_{RH} + MW_{O2})/2 \quad (28)$$

B

$$MW_B = 2MW_{R*} \quad (29)$$

Q

$$MW_Q = MW_B \quad (30)$$

Products

$$MW_P = \frac{\frac{n}{m}MW_{CO_2} + MW_{H_2O} + p(1-\phi)MW_{O_2}}{q} \quad (31)$$

The Halstead et al. model[37] uses the following equation to calculate temperature:

$$\frac{dT}{dt} = \frac{1}{C_v n_{tot}}\left(Q_K + Q_L - \frac{n_{tot}RT}{V}\frac{dV}{dt}\right) \quad (32)$$

where C_v is the constant volume heat capacity, n_{tot} is the total number of moles in volume V, Q_L is the heat loss through the boundary layer, and Q_K is the chemical energy release due to exothermic oxidation of the fuel. Q_L and Q_K are given by:

$$Q_L = \delta V(T - T_w) \quad (33)$$

where $\delta = \alpha S/V$ and α is the heat transfer coefficient and S/V is the surface to volume ratio.

$$Q_K = k_p hV[R*] \quad (34)$$

where h is the exothermicity. For the specific value of the CO_2/CO ratio used in the Halstead et al. model, an exothermicity of 394 kJ/mol is used for primary reference fuels (PRF) 70, 90, and 100.[37] The exothermicity represents the heat release per cycle due to the removal of $1/m$ units of fuel (i.e., $C_{n/m}H_2O_{k/m}$) per cycle.[37] The exothermicity of an oxygenated hydrocarbon can be estimated from the heat of formation of the fuel molecule, together with the CO_2/CO ratio of the products, which depends on the stoichiometry of the reaction. The heat of formation of methyl butanoate has been calculated to be in the range of 460.1−497.2 kJ/mol.[51−53] Therefore if the CO_2/CO ratio used in the work by Halstead et al. is kept constant (1:2, CO_2/CO) the exothermicity value of methyl butanoate is estimated to be ~350 kJ/mol. As all of the experimental points used in this work were either lean or stoichiometric, the CO_2/CO ratio was in the range of ~4:1 (stoichiometric) to more than 100:1 (Φ = 0.5), therefore the exothermicity was recalculated and determined to be in the range of 480−540 kJ/mol. However, it should be pointed out that although the exothermicity plays an important role in determining the end product temperature and pressure, it has little effect on the ignition delay, which is the focus of this study.

Since the last two terms of eq 32 are accounted for by the enthalpy transfer equation in CFD codes, only the contribution of the chemical reactions to the change in temperature needs to be calculated and can be described by:

$$\frac{dT}{dt} = \frac{1}{C_v n_{tot}}k_p hV[R*] \quad (35)$$

Schapertons and Lee[50] also increased the heat release by a factor of ($\Lambda + 1$) to account for the increased fuel consumption due to the modification of the propagation cycle. Therefore:

$$\frac{dT}{dt} = \frac{(\Lambda+1)}{C_v n_{tot}}k_p hV[R*] \quad (36)$$

The reaction rates above 950 K were frozen to their values at this temperature even if the actual temperature was higher as suggested by Schapertons and Lee.[50]

The concentrations of the species involved in the reactions can be solved by numerically integrating the differential equations for their rates of change. With the modifications suggested by Schapertons and Lee[50] and Hamosfakidis and Reitz[38] the rate of change of the species concentrations are described by:

$$\frac{d[R*]}{dt} = 2(k_q[RH][O_2] + k_B[B] - k_t[R*]^2) - f_3k_p[R*] \quad (37)$$

$$\frac{d[B]}{dt} = f_1k_p[R*] + f_2k_p[Q][R*] - k_B[B] \quad (38)$$

$$\frac{d[Q]}{dt} = f_4k_p[R*] - f_2k_p[Q][R*] \quad (39)$$

$$\frac{d[O_2]}{dt} = -pk_p[R*] \quad (40)$$

$$[RH] = \frac{[O_2] - [O_2]_{(t=0)}}{pm} + [RH]_{(t=0)} \quad (41)$$

where [M] is the molar concentration of species M.

With the above modifications to the model, it is possible to simulate cool flames, two-stage ignition, and the variation of

(51) Castro, E. A. *J. Mol. Struct. (Theochem)* **1995**, *339*, 239–242.
(52) Allinger, N. L.; Schmitz, L. R.; Motoc, I.; Bender, C.; Lamanowski, J. *J. Comput. Chem.* **1992**, *13* (7), 838–841.
(53) Afeefy, H. Y.; Liebman, J. F.; Stein, S. E. In *NIST Chemistry WebBook, NIST Standard Reference Database Number 69*, Linstrom, P.J., Mallard, W.G., Eds.; National Institute of Standards and Technology: Gaithersburg MD, 20899; http://webbook.nist.gov.

ignition delay with temperature in both lean and stoichiometric mixtures.

The application of the above multistep model to new fuels can be accomplished by modifying the 26 model constants. The model has been applied to diesel fuel in the past by using the 26 model constants suggested by Halstead et al.[37] for PRF 90 but with the adjustment of parameter A_{f_4}.[42,45,54] Hamosfakidis and Reitz also developed a genetic algorithm optimization methodology to determine the 26 Shell Model parameters for n-heptane (C_7H_{16}) and tetradecane ($C_{14}H_{30}$), guided by experimental results.[38]

Heat Loss Model

The RCM ignition modeling was achieved by incorporating the zero-dimensional multistep kinetic model with a heat loss model. Mittal and Sung[33,55] showed that the results of zero-dimensional modeling based on an approach of effective volume performs well in adequately predicting ignition delay, when there is a well-defined homogeneous adiabatic core within the RCM. Mittal and Sung's[33,55] method involves first estimating the heat loss by conducting a nonreactive experiment by compressing an inert mixture with the same specific heat and under the same operating condition as the reactive mixture. Using the nonreactive pressure results, the empirical heat loss parameters can be derived by using a specific heat loss model. This nonreactive pressure history can also be used to determine the time-dependent effective volume of the core region. This type of heat loss modeling is considered adequate if the simulated and experimental pressure traces for the nonreactive case match, with an example of this shown in Figure 5. Following this, the reactive experiment can be modeled using the same heat loss parameters.

The piston velocity during the compression stroke is required for the simulations and is based on the measured pressure traces. The index of polytropic compression (n), which is taken as a constant, is approximated from:

$$\frac{P_c}{P_0} = CR^n \tag{42}$$

where P_c and P_0 are the compressed and initial pressure, respectively, and CR is the compression ratio. Once n is calculated, the volume of the combustion chamber during compression, $V(t)$, can be written as:

$$V(t) = V_0\left[\frac{P_0}{P(t)}\right]^{1/n} \tag{43}$$

where V_0 is the initial volume, $P(t)$ is the experimental pressure trace. The velocity of the piston during compression, Vel(t) can then be calculated from:

$$\mathrm{Vel}(t) = \frac{\frac{dV(t)}{dt}}{\pi r^2} \tag{44}$$

where r is the piston radius and $dV(t)/dt$ is the rate of change in the chamber volume. The calculated piston velocity based on this method[33,55] for an example Michigan State University RCM run is shown in Figure 6. It can be seen that the piston accelerates until it reaches a peak velocity when approaching the end of its stroke near TDC. The piston then rapidly but uniformly decelerates. The calculated velocity profile shown in Figure 6 was also the piston velocity used for all of the modeling presented in this paper.

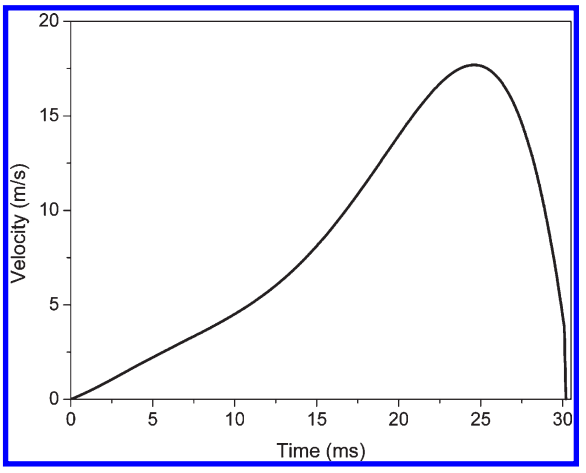

Figure 6. Piston velocity profile deduced from MSU RCM experimental data and used in modeling.

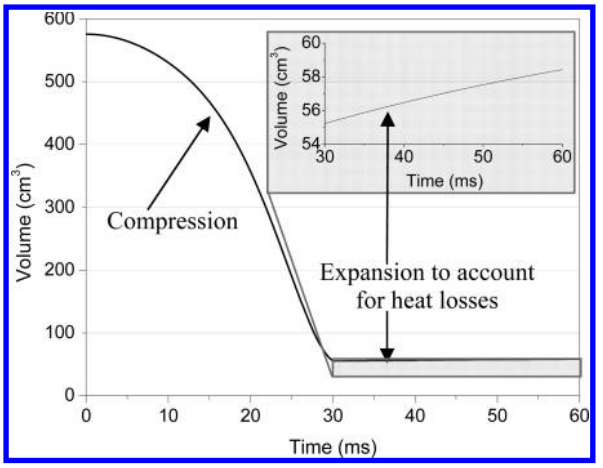

Figure 7. RCM combustion chamber effective volume used in modeling, including expansion after TDC (inset) to account for heat losses to chamber walls.

For the zero-dimensional modeling simulations, the compression stroke and the heat loss during the compression and post compression periods are accounted for with an approach based on volume expansion and determining the time-dependent effective volume of the core region.[33,55] Mittal and Sung[33] determined the effective volume of the core region, V_{eff}, by adding an empirically determined parameter V_{add} to the actual time dependent geometric volume of the combustion chamber, $V_g(t)$ so that the simulated pressure at the end of the compression stroke matches the experimental value, P_c. Therefore, V_{add} accounts for the effect of heat loss during compression. Following the end of compression, the volume expansion is expressed as a tenth order polynomial fit $v_p(t)$. The effective volume after TDC is equivalent to the product of the effective volume at TDC, $V_{eff}(t_{TDC})$ and the fitted volume expansion term, $v_p(t)$.

$$V_{eff}(t) = V_g(t) + V_{add} \quad t \le t_{TDC} \tag{45}$$

$$V_{eff}(t) = V_{eff}(t_{TDC})V_p(t) \quad t > t_{TDC} \tag{46}$$

V_{add} and $v_p(t)$, determined from the pressure history of the nonreactive mixture experiment, are the key parameters for

(54) Theobald, M. A. 1986, MIT.
(55) Mittal, G.; Raju, M. P.; Sung, C.-J. *Combust. Flame* **2008**, *155* (3), 417–428.

Table 2. Mixture Composition, Temperature, and Pressure of CHEMKIN Simulations

mix	Φ	MB (mole fraction)	O_2 (mole fraction)	N_2 (mole fraction)	T_c (K)	P_c (atm)
1	1	0.0313	0.2034	0.7653	738−940	23
2	0.5	0.0159	0.2067	0.7774	760−950	5.75, 11.5, 23, 46

the volume expansion model. These parameters can be used to generate the time varying effective volume profile shown in Figure 7, which is used to simulate the reactive mixture case using both the multistep model and the closed homogeneous reactor model in CHEMKIN 4.1, discussed further below.

CHEMKIN Model

Detailed chemical kinetic calculations were completed using the CHEMKIN code with a 0-D closed homogeneous reactor model.[56] A volume profile representing the piston compression in the RCM and accounting for the effect of heat loss, simulated as a process of adiabatic expansion, was incorporated. By taking this into account, the calculated pressure, temperature, and species concentrations can be compared with experimental RCM data. The volume profile used for the CHEMKIN modeling was identical to that used in the multistep autoignition modeling, discussed previously, and is shown in Figure 7.

The methyl butanoate mechanism of Dooley et al.,[1] which contains 275 species and 1545 reactions, was used for all CHEMKIN simulations. This mechanism was validated using shock tube and RCM autoignition measurements made by the authors,[1] together with speciation data available in the literature from a flow reactor, jet-stirred reactor, and opposed flow diffusion flame. The resulting mechanism is valid over a temperature range of 600−1700 K and a pressure range of 1−40 atm.[1] The authors note that the simulation of RCM ignition delays with the mechanism is less accurate than that for shock tubes, although the results do qualitatively agree. The authors attribute this to the error in experimentally measured ignition delay time, as they found that ignition delay times shorter than 50 ms were reproducible to within ±4 ms, but those greater than 50 ms were less reproducible. This is a result of the increasing effect of heat losses to the walls as the ignition delay time increases.[1] The methyl butanoate mechanism does not include low temperature chemistry to describe for example the isomerization of alkylperoxy radicals to hydroperoxyl radicals, as no negative temperature coefficient behavior was observed for methyl butanoate in the experiments.[1] However, in general, the longer chain methyl-esters components of biodiesel do show negative temperature coefficient behavior.[1]

Over 30 CHEMKIN simulations of methyl butanoate RCM ignition were completed in order to attain sufficient data with which to calibrate the multistep model. The pressure, temperature, and equivalence ratio of the simulations were chosen to be similar to those tested by Dooley et al.,[1] in order to ensure that the model could correctly predict the ignition delay, and in all cases results were comparable. The conditions tested with the CHEMKIN model are shown in Table 2.

(56) Kee, R. J.; F.M.R., Miller, J. A.; Coltrin, M. E.; Grcar, J. F.; Meeks, E.; Moffat, H. K.; Lutz, A. E.; G. Dixon-Lewis, Smooke, M. D.; Warnatz, J.; Evans, G. H.; R.S.L., Mitchell, R. E.; Petzold, L. R.; Reynolds, W. C.; Caracotsios, M.; Stewart, W. E.; Glarborg, P.; Wang, C.; McLellan, C. L.; Adigun, O.; W. G.H., Chou, C. P.; Miller, S. F.; Ho, P.; Young, P. D.; Young, D. J.; Hodgson, D. W.; Petrova, M. V.; Puduppakkam, K. V. Reaction Design: San Diego, CA, 2006.

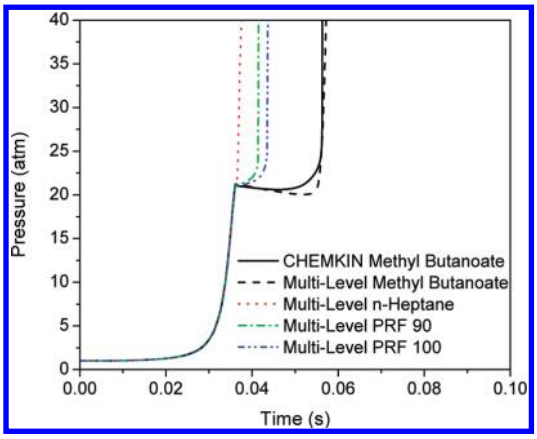

Figure 8. Comparison of methyl butanoate pressure traces with CHEMKIN and with the derived 26 model parameters, in addition to n-heptane,[38] PRF 90,[37] and PRF 100[37] using published constants (T_c = 825 K, P_c = 23 atm, and Φ = 1).

Fitting Procedure

As mentioned previously, the multistep model contains 26 model parameters that can be tailored to model a particular fuel. The model parameters include the activation energy, the pre-exponential factor, A, and the exponents x and y of the reaction rate equation for each of the reactions in the model:

$$\text{rate} = A\, e^{\left(\frac{-E_a}{RT}\right)}[X]^x[Y]^y \quad (47)$$

Although the 26 parameters are adjustable to each fuel, there is kinetic information available concerning the rates of the chain propagation steps, which are related to alkylperoxy isomerization theory.[37] Thus, the values of A_{p1}, E_{p1}, A_{p2}, E_{p2}, A_{p3}, and E_{p3} used here were those gathered by Halstead et al.[37] from literature data and were not altered, as although methyl butanoate shows only single stage ignition, other longer chain methyl-esters components of biodiesel do show negative temperature coefficient behavior.[1] Starting from the PRF 90 and PRF 100 parameters published by Halstead et al.,[37] the remaining 20 constants were individually increased and decreased to determine their effect on the ignition delay and this information was then used to match the ignition delay found from the CHEMKIN modeling.

Figure 8 shows a comparison of the CHEMKIN methyl butanoate pressure trace together with traces calculated using the 26 constants suggested by Hamosfakidis and Reitz[38] for n-heptane, and those suggested by Halstead et al.[37] for PRF 90 and PRF 100. The multilevel methyl butanoate pressure trace is that attained using the 26 multistep model constants determined in this work. All results are for an equivalence ratio of 1, compressed temperature of ∼822 K, and a compressed pressure of 23 atm. From the figure it can be seen that the ignition delay of methyl butanoate is significantly longer than that of the other three fuels and for this reason 11 of the remaining 20 constants that could be potentially altered were changed. The task of determining appropriate constants was facilitated by the fact that methyl butanoate ignites in a single stage. The 26 model constants determined for methyl butanoate, in addition to the PRF 90 and PRF 100 constants

Table 3. Multistep Model Constants for PRF 90,[37] PRF 100,[37] and Methyl Butanoate[a]

parameter	90 PRF	100 PRF	methyl butanoate
A_{p1}	1.0×10^{12}	1.0×10^{12}	1.0×10^{12}
E_{p1}	0	0	0
A_{p2}	1.0×10^{11}	1.0×10^{11}	1.0×10^{11}
E_{p2}	1.5×10^{4}	1.5×10^{4}	1.5×10^{4}
A_{p3}	1.0×10^{13}	1.0×10^{13}	1.0×10^{13}
E_{p3}	8.5×10^{2}	8.5×10^{2}	8.5×10^{2}
A_q	1.2×10^{12}	3.96×10^{13}	1.5×10^{10}
E_q	3.5×10^{4}	4.0×10^{4}	5.0×10^{4}
A_b	4.4×10^{15}	6.512×10^{15}	6.512×10^{15}
E_b	4.5×10^{4}	4.0×10^{4}	6.0×10^{4}
A_t	3.0×10^{12}	3.51×10^{12}	3.0×10^{5}
E_t	0	0	0
A_{f1}	7.3×10^{-4}	7.3×10^{-4}	9.3
E_{f1}	-1.5×10^{4}	-1.5×10^{4}	-1.5×10^{4}
A_{f2}	1.8×10^{2}	1.8×10^{2}	1.8×10^{2}
E_{f2}	-7.0×10^{3}	-7.0×10^{3}	-7.0×10^{3}
A_{f3}	1.47	2.205	1.205
E_{f3}	1.0×10^{4}	1.0×10^{4}	1.5×10^{4}
A_{f4}	1.88×10^{4}	1.7×10^{4}	1.88×10^{4}
E_{f4}	3.0×10^{4}	3.0×10^{4}	4.0×10^{4}
x_1	1.0	1.0	1.5
y_1	0	0	0
x_3	0	0	0
y_3	0	0	0
x_4	−1.0	−1.0	−0.3
y_4	0.35	0.35	0.35
n	7.9	8	5
m	8.9	9	5
k	0	0	2

[a] A_i (cm,mol,s units), E_i (cal/mol), R = 1.9872 cal/mol K.

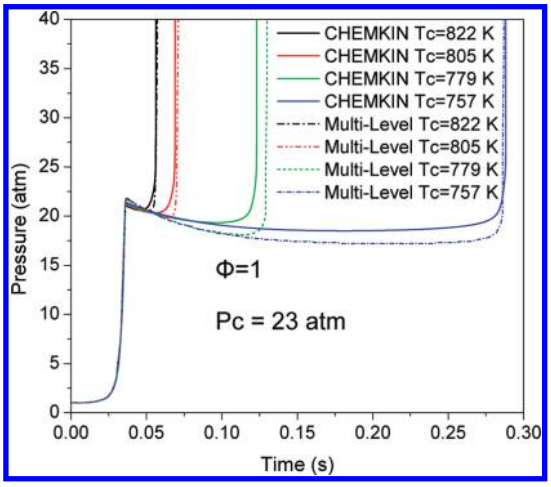

Figure 9. Pressure traces of the multistep and CHEMKIN modeling runs at different compressed temperatures (Φ = 1 and P_c = 23 atm).

published by Halstead et al.,[37] can be found in Table 3. In the future, it is planned to fit RCM experimental data of two-stage ignition fuels, such as biodiesel, using an optimization method that is currently under development.

Results and Discussion

Methyl butanoate multistep model pressure trace results together with those attained using CHEMKIN with the detailed methyl butanoate mechanism at Φ = 1 and a compressed pressure of 23 atm are shown in Figure 9. The multistep results show good agreement with those achieved with CHEMKIN, with the computational time reduced by more than 2 orders of magnitude. Additionally, it should be pointed out that, as anticipated, the CHEMKIN results compare well

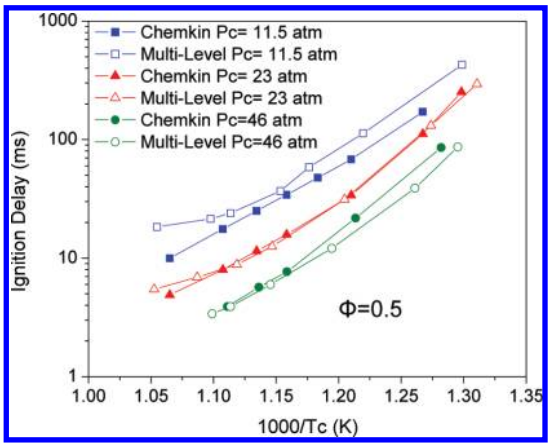

Figure 10. Methyl butanoate autoignition delay times with CHEMKIN (solid) and the multistep model (hollow) at Φ = 0.5.

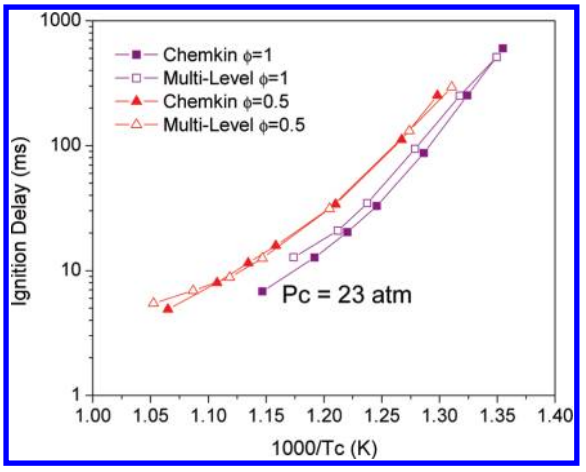

Figure 11. Methyl butanoate autoignition delay times with CHEMKIN (solid) and the multistep model (hollow) at P_c = 23 atm.

to those of Dooley et al.[1] as their detailed kinetic mechanism was used.

A comparison between the ignition delay achieved with the multistep model and that using CHEMKIN is shown in Figures 10 and 11. In Figure 10 the effect of increasing compressed pressure on ignition delay is visible at a constant equivalence ratio of 0.5. It can be seen that the multistep model correctly simulates the increase in ignition delay that occurs with decreasing compressed pressure for an equivalent compressed temperature.

Figure 11 shows the effect of different equivalence ratios on ignition delay at a compressed pressure of 23 atm. In this case, it is observable that the multistep model adequately predicts the decreased ignition delay that arises as the equivalence ratio changes from 0.5 to stoichiometric for a given compressed temperature. In all cases shown in Figures 10 and 11, the ignition delay decreases with increasing compressed temperature.

Contours showing percent error in the predicted ignition delay of the multistep model relative to the CHEMKIN results for the conditions shown in Figure 10 are visible in Figure 12. From the figure it can be seen that at higher compressed temperatures the multistep model overpredicts the ignition delay, relative to the CHEMKIN model, whereas at lower compressed temperatures the ignition delay is underpredicted. There are also some discrepancies in the ignition

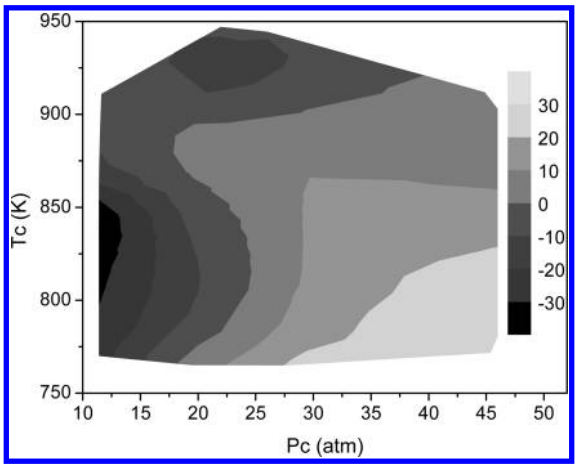

Figure 12. Contours of percent error of the ignition delay prediction between the multistep model and CHEMKIN results for $\Phi = 0.5$.

delay at the highest and lowest temperatures tested, which is also visible in Figures 10 and 11.

The average relative error in the predicted ignition delay when using the multistep model relative to CHEMKIN for all of the conditions shown in Figures 10 and 11 was found to be 14.9%. However, if the error in the experimental RCM ignition delay mentioned by Dooley et al.[1] is taken into account; the error between the CHEMKIN and multilevel model results is reduced to less than 7%. In the future, it is expected the error may be further reduced through optimization of the 26 model parameters using the previously mentioned optimization code. In addition, it is projected that optimization will be necessary for fuels that undergo two−stage ignition.

Conclusions

A multistep model was adapted for use with oxygenated fuels, with focus on the biodiesel surrogate fuel, methyl butanoate. The preliminary results presented in this paper indicate the feasibility of using this type of multistep modeling to simulate two-stage ignition of oxygenated hydrocarbons and their blends over a range of operating conditions possible in a RCM. The results of using the adapted multistep model with the 26 model constants fitted specifically for methyl butanoate compared well with the CHEMKIN modeling using the detailed kinetic model. Over the range of conditions tested, the percent relative error in the ignition delay between the multistep and CHEMKIN modeling was less than 15%. Discrepancies between the multistep modeling and CHEMKIN results were largest at the highest and lowest compressed temperatures. It is anticipated the error could be further reduced by optimizing the model constants using an optimization code. Such a method will be critical when determining constants for biofuels, the majority of which are two-stage ignition fuels. Future plans include experimental RCM testing of a range of oxygenate fuels and their blends in order to determine multistep model constants for the different fuels. In addition, the characteristics of blends of mixtures, most notably determining if it is possible to predict mixture characteristics based on the original components, will be examined. The availability of multistep model constants for a range of oxygenated fuels will be a valuable tool in dramatically reducing the computational time of autoignition modeling, especially in CFD applications.